A.A. Bespalko, D.D. Dann[*], M.V. Petrov, E.K. Pomishin

National Research Tomsk Polytechnic University, Russia,
([*]E-mail: dddann@tpu.ru)

Acoustic-electrical testing of defects
in the cement-sand and cement-glass model samples

A complex method of acoustic-electrical testing of defects in dielectric samples made from cement-sand and cement-glass mixtures is discussed. The paper reports the results of studies of changes in the parameters of electromagnetic responses and their spectra under pulsed deterministic acoustic excitation of model samples with defects in the form of solid-state inclusions. The results of mathematical calculations of the time variation in the stress-strain state induced in a defective dielectric model sample by deterministic acoustic pulse are presented. The relationship is shown between the parameters of the acoustic excitation and the electromagnetic response to the impact in a magnetic field. The study revealed that the specific electrical resistance of the cement-sand and cement-glass mixtures differs significantly. Excitation of electrical double layers by acoustic pulses causes an electromagnetic signal, parameters of which depend on the parameters of the acoustic impact and acoustic and electrical properties of the material. As a result, a reduced specific electrical resistance of the mixture increases its conductivity. The numerical calculation of the propagation of the deterministic acoustic pulse showed that its parameters change when it passes through a defect with acoustic impedance different from that of the mixture used.

Keywords: non-destructive testing, dielectrics, acoustic impact, electromagnetic radiation, magnetic field, modeling.

Introduction

At present, the increasing number of products is manufactured from solid dielectric materials and composites. These products are used in various conditions, including extreme ones. Insulators, structural dielectrics, concrete structures and other practically used dielectrics require regular non-destructive testing to be environmentally friendly. Early detection of defects in dielectric products is crucial to maintaining their mechanical and electric strength. The defects in solid materials and products are detected using well-proven non-destructive testing methods: ultrasonic, acoustic pulse and acoustic emission; electrical and electromagnetic; magnetic; X-ray and other methods [1–10]. This variety of non-destructive methods is not always efficient for testing of dielectric materials and structures. This is due to close values of the acoustic impedance of the media of the product and the defect during ultrasonic sounding and during acoustic emission testing of the fracture development; lack of magnetic properties in the majority of composites, including dielectric materials; high X-ray permeability in organic and some inorganic dielectrics, and dangerous effect of radiation on the operator's health. Therefore, complex destructive testing methods should be employed based on well-proven algorithms and newly developed ones. Mechanoelectric or acoustic-electrical [11–19] conversions in solid-state structures can be successfully used to develop such complex testing techniques. The acoustic-electrical test uses contact acoustic sounding of the test object and contactless recording of the electromagnetic response to this impact with further amplitude-frequency analysis of the electromagnetic signal. External acoustic deterministic pulses or acoustic pulses arising in

the material during fracture development induced by mechanical load can be used as a source of vibrations [11, 12]. As a result of this action, charges or electrical double layers at the interfaces of media, inclusions or blocks, on crack sides or on other structural defects of the dielectric materials emit electromagnetic signals.

A mathematical and physical rationale for testing dielectric heterogeneous materials by electromagnetic signal parameters is reported in [20]. It is shown that mechanical vibrations induced by a normalized single impact cause a displacement current. Experimental studies [21, 22] also indicate that the passage of acoustic waves causes EMS generation, which is associated with vibrations of electrical double layers. In this case, EMS amplitude-frequency parameters depend on the characteristics of acoustic pulses and the charge state of the defects in the form of inclusions.

Thus, under an external deterministic acoustic impact, defects in the form of solid inclusions or voids can be successfully tested with regard to the parameters of electromagnetic responses to this perturbation. The paper discusses the applicability of the acoustic-electric method of non-destructive testing for defective model composite dielectric materials made from cement-sand (CSM) and cement-glass (CGM) mixtures. Solid materials with acoustic impedance different from the impedance of the used CSM and CGM composites were used as defects.

Methods of conducting experiments

For experimental studies of the acoustic-electrical conversion samples were made from a cement-sand and cement-glass mixture with a size of $(50 \times 50 \times 95) \times 10^{-9}$ m^3 with artificial solid parallelepiped inclusions of different size (Fig. 1). The samples were fabricated in accordance with [22]. The moisture content of the samples did not exceed 1.5 % of the sample weight, the sand grain size was $(2.5-8.0) \times 10^{-4}$ m, and the size of glass fractions varied in the range of $(1.5-2.5) \times 10^{-4}$ m. For EMS measurements, the side sample surface of $(50 \times 95) \times 10^{-6}$ m^2 was laid out into 15 sites. The width of the EMS measurement sites depended on the size of the capacitive sensor lobe of the electromagnetic receiver.

A point impact with a ball weighing 8.59×10^{-4} kg was applied to the center of the sample end face with the area of $(50 \times 50) \times 10^{-6}$ m^2. The materials used as inclusions to simulate defects, are presented in Table 1. The materials were chosen to have their acoustic impedance and electrical resistivity greater or less than z and ρ of CSM or CGM.
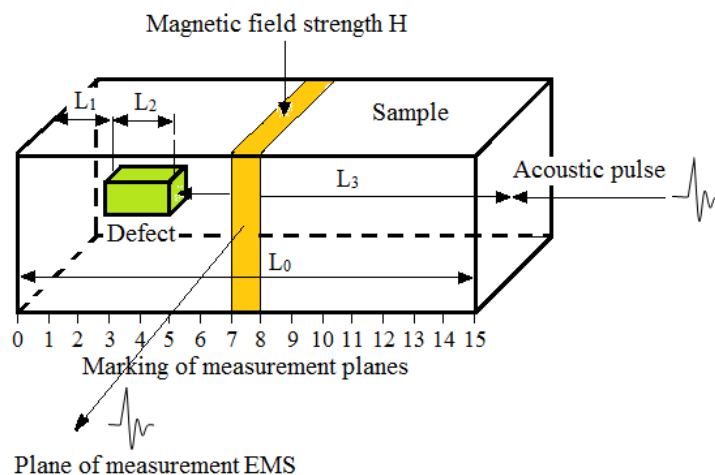

Figure 1. A model sample made from the cement-sand or cement-glass mixture with a solid rectangular inclusion with a magnetic field of strength *H* applied to the mixture material–defect contact

Four sizes of the rectangular defects used were $(1.0 \times 1.0 \times 1.5) \times 10^{-6}$ m^3, $(1.5 \times 1.5 \times 2.0) \times 10^{-6}$ m^3, $(2.0 \times 2.0 \times 3.0) \times 10^{-6}$ m^3, and $(2.5 \times 2.5 \times 3.8) \times 10^{-6}$ m^3. The axes of the defects were coaxial with the sample axes. The largest faces of the defects were parallel to the larger surfaces of the model samples. The sand/glass–cement ratio was two parts to one part by weight, and the water-cement ratio was 0.7. Before pouring the solution, the inclusions were fixed in the mold in the desired position using an elastic dielectric thread. After solidification, the samples were stored at $(20-22)^\circ$C for 28 days. The position of the inclusion in the sample was monitored by digital radiography using the PerkinElmer XRD 0822 detector [23]. Changes in the elec-

trical resistance R of the samples were measured at frequencies of (1–100) kHz using an LCR-819 immittance meter [24].

Acoustic and electrical parameters of the materials used

No.	Defect material	Specific gravity of the material ρ_v, kg/m^3	Longitudinal sound speed c_l, m/s	Acoustic impedance $z \cdot 10^6$, kg/s·m^2	Specific electrical resistance ρ, Ohm·m
1	Cement-sand mixture (CSM)	1900	2765	5.25	38.4×10^3
2	Cement-glass mixture (CGM)	1973	3240	6.39	14.7×10^3
2	Plexiglas (PMMA)	1200	2700	3.24	10^{17}–10^{18}
3	Fluoroplastic (PTFE)	2200	1340	2.95	10^{15}–10^{17}
4	Ebonite	1150	2400	2.76	10^{12}–10^{14}
5	Glass, flint	2500	4560	11.4	10^9–10^{12}
6	Magnetite Ore (75 %)	4150	5870	24.34	10^{-3}-10^2
7	Duralumin, D16T	2700	6400	17.28	2.8×10^{-8}
8	Brass, L59	8500	4600	39.10	6.5×10^{-8}
9	Carbon steel	7800	5890	45.94	1.3×10^{-7}

The resistance measurement error was 0.05 %. The specific electrical resistance of the mixtures was calculated by the formula

$$\rho = \frac{RS}{L}, \tag{1}$$

where R is the sample resistance, S is the area of the channel through which the current flows, L is the channel length. Graphs of ρ changes versus frequency for CSM and CGM are shown in Figure 2. Table 1 presents the value $\rho_s = 38.4 \times 10^3$ Ohm·m, which corresponds to the frequency of the highest amplitude in the EMS spectrum. At equal frequency CGM samples exhibit electrical resistivity $\rho_g = 14.7 \times 10^3$ Ohm·m.
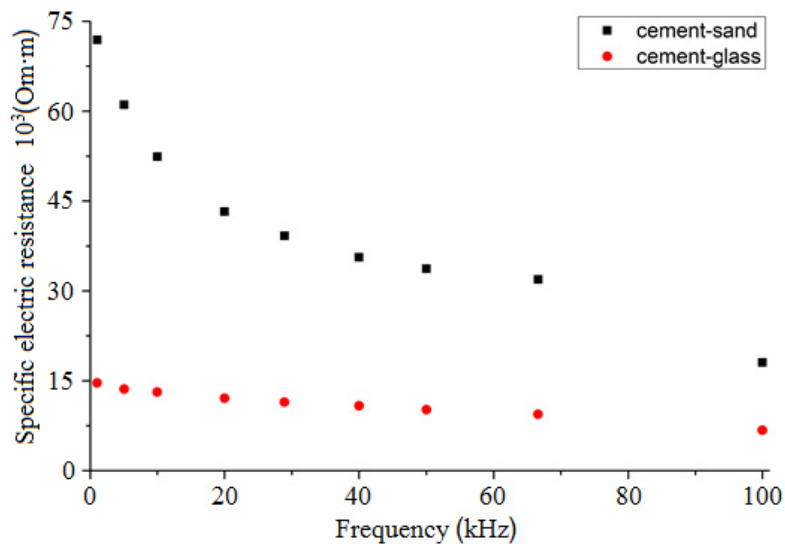

Figure 2. Changes in the specific electrical resistance of CSM and CGM samples

Figure 2 shows that the specific electrical resistance of CSM is lower than that of CGM in the entire range of the frequencies used. As shown below, this range corresponds to the frequency range of the recording capacitive differential sensor (EDS). The block diagram of the stand used for acoustic excitation and recording of the sample electromagnetic response to this impact is shown in Figure 3. It includes a dynamic acoustic pulse excitation system AP, a system for receiving and measuring the parameters of electromagnetic responses EMS. The energy of the acoustic pulse was monitored by measuring the velocity of the impact ball flight through two optical pairs that consisted of LED and a photodiode. The AP shape was monitored using a broadband piezoelectric receiver [25]. The measurement data were transmitted from the NI BNC 2120 unit

[26] or from the Tektronix 2024B oscilloscope to the computer for further amplitude-frequency analysis using the developed and standard programs.
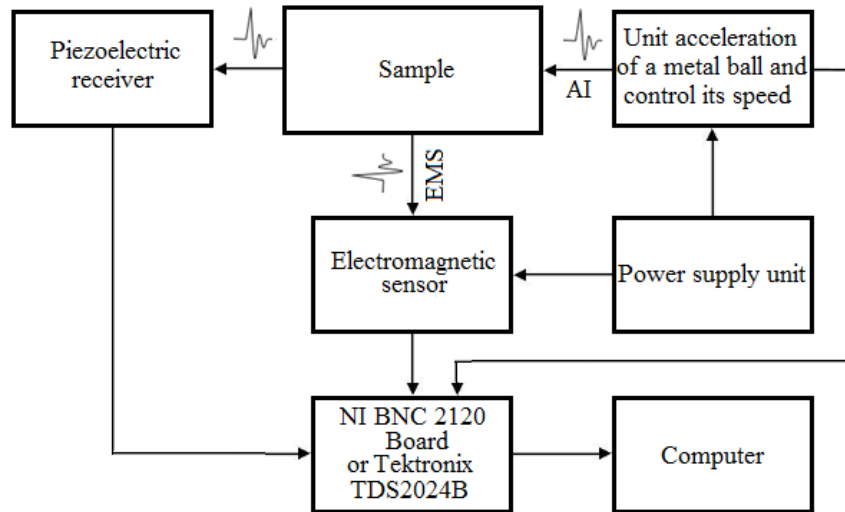

Figure 3. Block diagram of the stand for acoustic excitation
of electromagnetic signals in the test model samples

In the dynamic acoustic pulse excitation system, a spring device was used to accelerate the ball. The ball hit a hardened steel plate 2.5×10^{-3} m thick with an acoustic impedance z and hardness close to z_b of the ball, which was in acoustic contact with the sample. The velocities of the flight and rebound of the ball were determined using two optical pairs that included a light emitting diode LED and a photodiode PD installed at a distance of 5×10^{-2} m from each other. The impact excited an acoustic signal of certain amplitude and time parameters in the plate. From the plate, the acoustic pulse passed through a layer of mineral oil into the test sample. Mineral oil was also used to provide the acoustic contact of the sample with a piezoelectric receiver of the acoustic signals transmitted through the sample. The primary acoustic pulse excited by the ball was close to a bell-shaped one, and its base duration was 50×10^{-6} seconds. Analog signals from the measuring system of the ball flight were fed to the measuring eight-channel NI BNC-2120 module. After that, the EMS was transmitted to the computer. The battery pack provided 6V voltage across the LED and PD of the measuring system. The ball velocity at the moment of impact V_i^2 and that of the rebound from the target V_b^2 were calculated with regard to the time of the ball flight and the distance between the optoelectronic pairs. The obtained values of the velocity and the ball mass (m), as well as the approximation of elastic collision of the ball with the grounded metal plate were used to calculate the acoustic impact energy transmitted to the sample as

$$E_{exc} = \frac{m}{2}\left(V_i^2 - V_b^2\right), \qquad (2)$$

where E_{exc} is the energy induced in the sample upon ball impact. The energy losses of the acoustic pulse in the plate were not considered. The spring compression was changed to induce the acoustic impact energy in the test sample within $(8-30) \times 10^{-3}$ J. The longitudinal speed of sound was measured with a piezoelectric emitter using the same stand (Fig. 3).

EDS operating in the range from 1 to 100 kHz was used as a receiver of electromagnetic signals. At the output of the capacitive sensor, the signal could be amplified 10 or 100 fold. The EDS input sensitivity was 5×10^{-4} V. The size of the receiving plates of the sensor was $(0.5 \times 3.0) \times 10^{-4}$ m^2. During the experiments, the distance from the surface of the test samples to the nearest plate of the electromagnetic sensor was set within $(1-2) \times 10^{-3}$ m. The electromagnetic sensor for measuring electromagnetic signals along the entire sample length was enabled to move along its central axis sequentially over the measurement sites from 0–1 to 14–15 and backwards. The initially set distance between the receiving plate of the electromagnetic sensor and the sample surface was maintained stable during EMS measurements using the optical stage dials and the control plate of a given thickness. A special program was used to normalize EMS to the perturbation created by the ball impact, and the fast Fourier transform (FFT) program was used to perform its spectral analysis.

Theoretical and experimental research

Numerical and experimental modeling was carried out for testing CSM and CGM model samples, including those with rectangular defects. Initially, numerical modeling was performed using the concept of continuum mechanics for elastic wave propagation in a dielectric sample under excitation by deterministic acoustic pulses. The computational algorithm for determining the parameters of the stress-strain state (SSS) of the model sample is based on the relations of the mechanics of the deformed body. In the general case, a system of equations was used, describing the behavior of a deformable solid in space and includes well-known equations, continuities, and relations between the components of the total strain rate tensor. In addition, the calculations employed the constitutive relations that specify the relationship between the components of the stress and strain tensors:

$$\sigma_{ij} = f(\varepsilon_{ij}), \tag{3}$$

$$\varepsilon_{ij} = \frac{\Delta x_{ij}}{x_{ij}}, \tag{4}$$

where x_{ij} is spatial coordinates; σ_{ij} is stress tensor components; ε_{ij} is total strain tensor components.

The numerical implementation was carried out according to a noncentral difference scheme of the second order of accuracy with respect to the space and time steps [27]. The accuracy of the numerical results was assessed by the internal convergence of the results when changing the parameters of the finite-difference grid and time integration steps [28]. The boundary conditions were set in accordance with the laboratory experiments. In calculations, the excitation corresponded to the experiment acoustic pulse in shape, amplitude, and duration. The calculations were performed for the sample $(5.0 \times 5.0 \times 9.5) \times 10^{-6}$ m^3 in size with real elastic properties. For calculations, the following values of CGM properties were set: density of $(1.9–2.3) \times 10^3$ kg/m^3; modulus of elasticity of 4×10^{10} N/m^2; Poisson's ratio of 0.2; longitudinal wave velocity of 3.2×10^3 m/s. The calculation was performed for the impact onto the center of the sample end face. An elastic calculation model was used. The numerical simulation results were visualized using a special graphics package.

Figure 4 presents the results of modeling the perturbation propagation over the simulated region. The results were visualized as isosurfaces. At time 5×10^{-6} s (Fig. 4a), perturbation propagates over the homogeneous region in the form of a hemisphere, which corresponds to the general concepts of the mechanics of acoustic wave propagation. For clarity, the interaction between the wave front and a carbon steel insert with sizes of $(2.5 \times 2.5 \times 3.8) \times 10^{-6}$ m^3 was considered. Figure 4b shows how the leading edge of the wave meets a harder insert and bends it at lateral sides. At the next propagation stage, the wave front moves faster along a more elastic insert, Figure 4c.
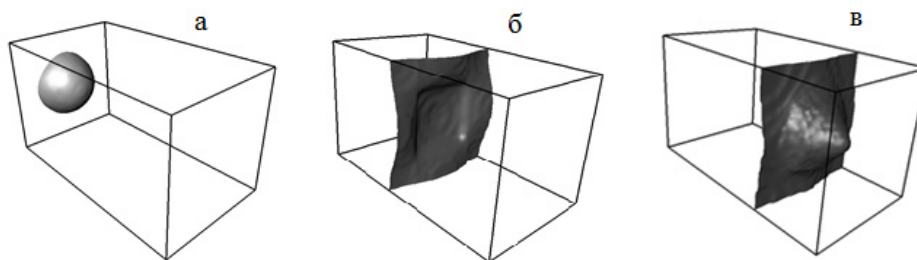

Figure 4. Propagation of elastic perturbation in the model in time:
a) 5×10^{-6} s; b) 10×10^{-6} s; c) 12×10^{-6} s.

Thus, the inserts with elastic properties different from those of the base material change the of the wave process pattern. Changes in the elasticity modulus and material density produce the greatest effect. For example, the ratio of the elasticity moduli of carbon steel and the base material differs more than 10 fold. The smaller the difference in elasticity moduli, the less sensitive the wave process to inhomogeneities. The sums of rates were calculated for carbon steel, fluoroplastic, magnetite ore, and glass (flint) defects of various sizes. Figure 5 presents the example of the calculated changes in the integral characteristics of the sums of displacement rates in layers of CSM (Fig. 5, a, b, c) and CGM (Fig. 5, d, e, f) that are close to 75 % magnetite

ore defects of sizes: $(1.0×1.0×1.5)×10^{-6}$ m^3, $(2.0×2.0×3.0)×10^{-6}$ m^3, $(2.5×2.5×3.8)×10^{-6}$ m^3. The figure shows that the displacement rates change significantly in layers close to defects of different sizes. As reported in [10–22], the parameters of acoustic excitation and electromagnetic response to this type of impact are uniquely related, therefore, the parameters of the recorded EMS will be close to the changes in the sums of rates shown in Figure 5.

The calculations in Figure 5 show that an increase in the defect size shifts the spectrum towards the high-frequency region.
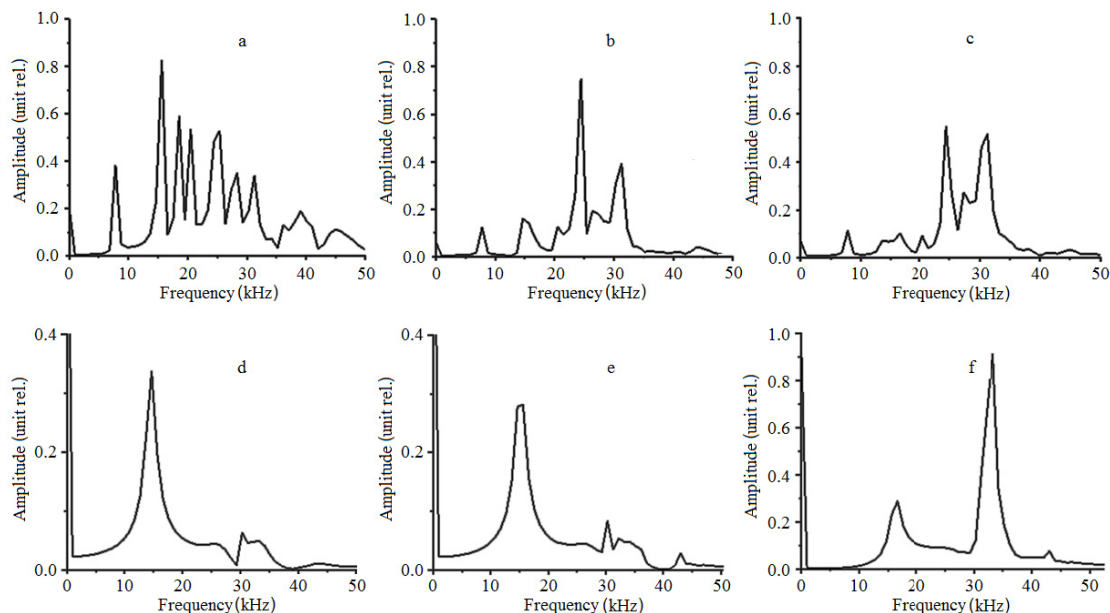
Figure 5. Calculated integral characteristics of the sums of displacement rates in layers close
to 75 % magnetite ore defects of different sizes: a, d) $(1.0×1.0×1.5)×10^{-6}$ m^3;
b, e) $(2.0×2.0×3.0)×10^{-6}$ m^3; c, f) $(2.5×2.5×3.8)×10^{-6}$ m^3; a, b, c for CSM; d, e, f for CGM

Further experimental studies were performed for electromagnetic signals and their spectra excited by deterministic acoustic pulses in CSM and CGM samples with steel, carbon steel, fluoroplastic, magnetite ore, and glass (flint) defects. In the experiments an acoustic pulse was applied to the center of the sample end face, and the receiving electric sensor was located near the lateral surface at a distance of at least 10^{-2} m from the impact point at a height of $2×10^{-3}$ m. A magnetic field was applied to samples with magnetizable defects, which corresponded to strength $H = 1.45×10^5$ A/m on the sample surface (Fig. 1). The magnetic field was applied to samples made from different model mixtures (CSM and CGM) to reveal its effect on the amplitude of EMS from magnetizable defects. Previous experiments on the 75 % magnetite ore samples [29] showed that under acoustic excitation the applied magnetic field significantly affects the electromagnetic responses.

Initially, the studies were conducted for CSM and CGM samples with a ferrite magnet defect $(1.0×1.0×1.5)×10^{-6}$ m^3 in size without magnetic field and with magnetic field of $1.45×10^5$ A/m applied to the sample surface. Figure 6 shows electromagnetic signals and their spectra under deterministic acoustic excitation of the CSM sample with a ferrite magnet defect with sizes of $(1.0×1.0×1.5)×10^{-6}$ m^3 without magnetic field (Fig. 6 a, c) and with magnetic field of $1.45×10^5$ A/m applied to the sample surface (Fig. 6 c, d). The figure shows that when magnetic field is applied, the EMS amplitude and spectral components increase by more than 20 %. That increase was observed in all EMS measurements during excitation with acoustic pulses with similar acoustic pulse amplitudes. In addition, the figure shows a good correlation between the EMS spectra in both cases.

Figure 7 shows changes in the EMS amplitude and spectra for CGM samples, which have a lower specific electrical resistance (Fig. 2) with the defect similar to that in CSM samples. In Figure 7, the EMS amplitude and spectra of CGM samples are significantly lower than the amplitude and spectra of CSM samples. Moreover, magnetization decreases the amplitudes and spectral components of the signal.
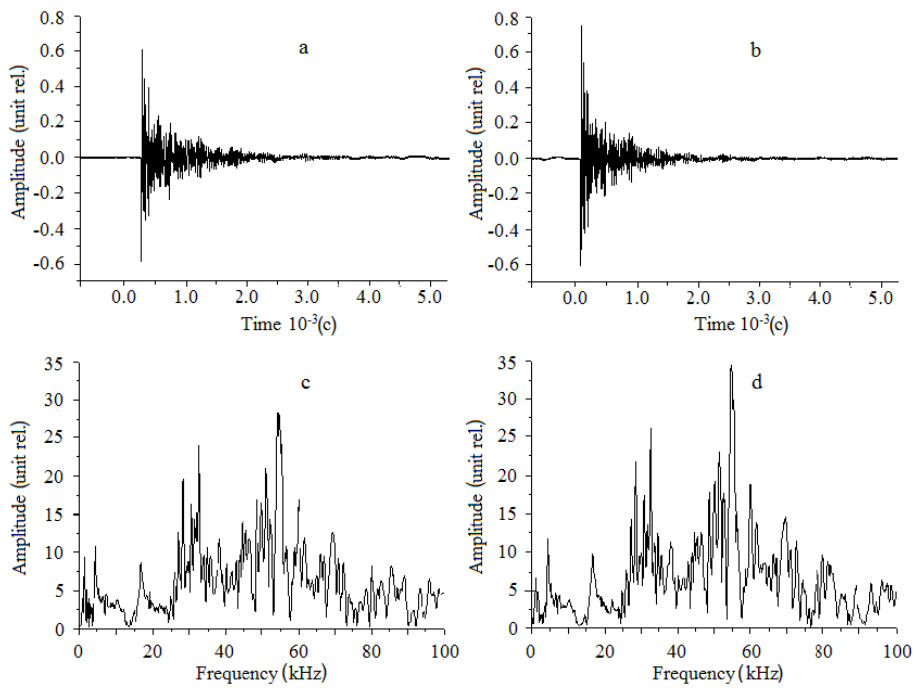
Figure 6. Electromagnetic signals and their spectra upon deterministic acoustic excitation of CSM sample with a ferrite magnet defect with sizes of $(1.0 \times 1.0 \times 1.5) \times 10^{-6}$ m^3 without magnetic field (a, c) and with magnetic field of 1.45×10^5 A/m applied to the sample surface (b, d)
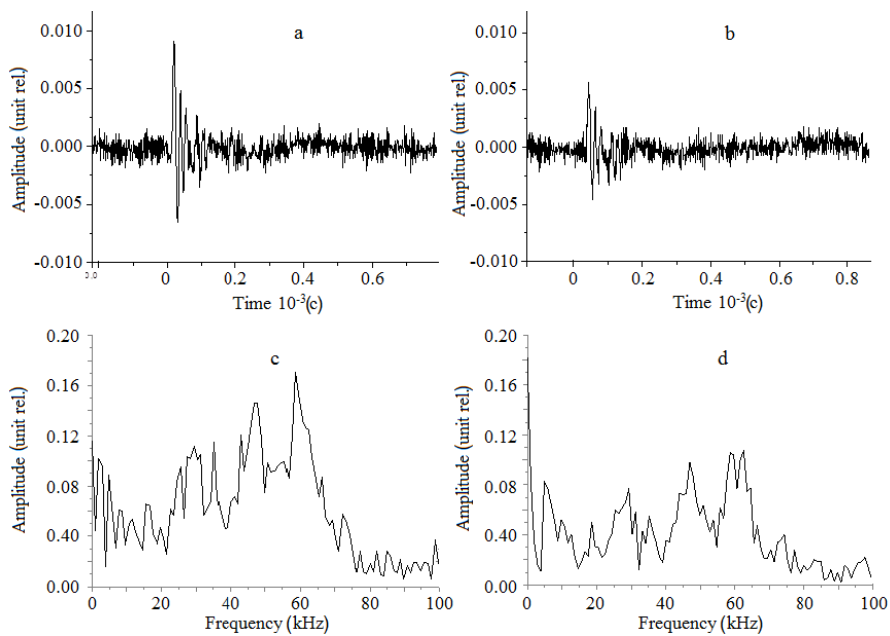

Figure 7. Electromagnetic signals and their spectra upon deterministic acoustic excitation of the CGM sample with a ferrite magnet defect $(1.0 \times 1.0 \times 1.5) \times 10^{-6}$ m^3 in size without magnetic field (a, c) and with magnetic field of 1.45×10^5 A/m applied to the sample surface (b, d)

Addition of a 75 % magnetite ore defect in the CSM sample showed that the EMS amplitude and spectra in these samples without magnetic field and with magnetic field applied tend to decrease (Fig. 8) similar to previous experiments.
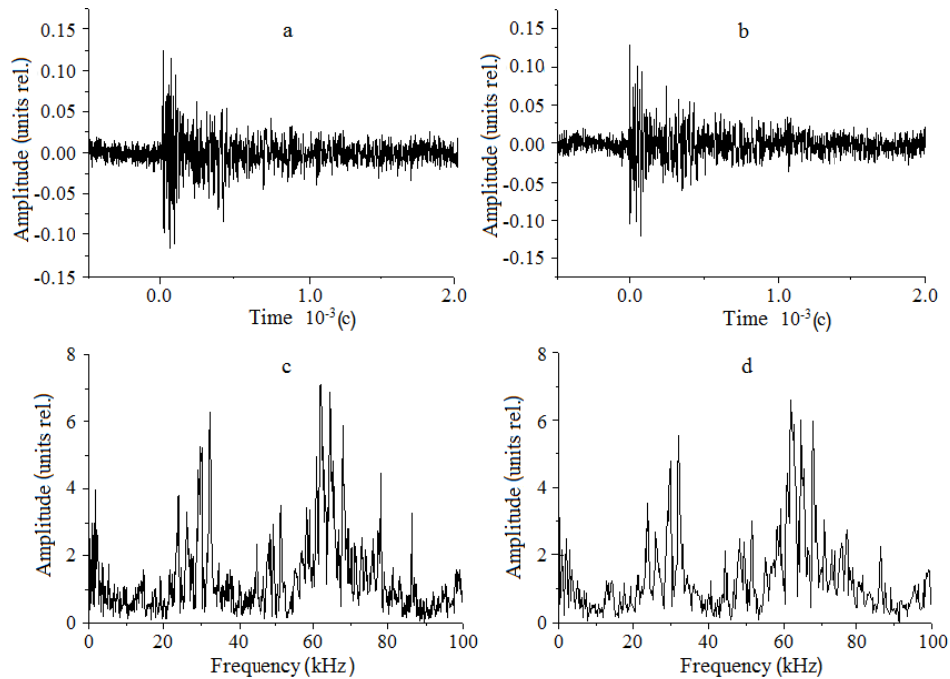
Figure 8. Electromagnetic signals and their spectra upon deterministic acoustic excitation of the CSM sample with magnetite defect with s of $(1.0 \times 1.0 \times 1.5) \times 10^{-6}$ m^3 without magnetic field (a, c) and with magnetic field of 1.45×10^5 A/m (b, d) applied to the sample surface

Discussion and conclusions

The study revealed that the specific electrical resistance of the cement-sand ρ_{csm} and cement-glass ρ_{cgm} mixtures differs significantly (Fig. 2). In addition, the acoustic impedance z of mixtures and defects in the mixture differs (Table 1). This has a significant effect on the parameters and propagation of deterministic acoustic pulses in defective samples and on the parameters of the electromagnetic responses excited at the contact between the sample and the defect materials during acoustic-electrical conversions [19]. Excitation of electrical double layers (EDL) by acoustic pulses causes an electromagnetic signal, parameters of which depend on the parameters of the acoustic impact and acoustic and electrical properties of the material [10–19]. As a result, a reduced ρ of the mixture increases its conductivity. In turn, increased conductivity facilitates the drainage of the EDL charge generated at the contact between the materials of the mixture and the defect. Then, the EMS amplitude decreases proportionally under the acoustic impact on the electrical double layer. In this case, the applied magnetic field leads to the polarization of magnetic dipoles and, therefore, to the drainage of a weakly fixed EDL charge under the action of Lorentz forces. The results of weakening of the EMS signal amplitudes and its frequency components were significant for CGM samples with a ferrite magnet defect (Fig. 7) and insignificant for CSM samples with a 75 % magnetite ore defect (Fig. 8). At the same time, the amplitude of EMS and its spectral components in CSM samples with a ferrite magnet increased significantly. This can be attributed to better dielectric properties of CSM as compared to CGM (Table 1) and, as a result, an increased EDL charge.

Thus, the numerical calculation of the propagation of the deterministic acoustic pulse showed that its parameters change when it passes through a defect with acoustic impedance different from that of the mixture used. The obtained integral characteristics of the sums of the displacement rates in layers close to carbon steel defects with sizes of $(1.0 \times 1.0 \times 1.5) \times 10^{-6}$ m^3, $(2.0 \times 2.0 \times 3.0) \times 10^{-6}$ m^3, and $(2.5 \times 2.5 \times 3.8) \times 10^{-6}$ m^3 differ significantly.

Experimental studies of EMS and its spectral components in CSM and CGM samples showed that samples with high electrical resistivity show more stable amplitude-frequency characteristics of electromagnetic signals under similar deterministic acoustic excitation. An increase or retention of EMS characteristics can also be observed when a magnetic field is applied to defective CSM samples.

Acknowledgements

References

1 Mason W.P. Physical Acoustics. — V. 1 / W.P. Mason. — New York: Academic Press, 1964. — 532 p.

2 Клюев В.В. Неразрушающий контроль. / В.В. Клюев. — Т. 3 — М.: Машиностроение, 2008. — 864 с.

3 Blitz J. Electrical and Magnetic Methods of Non-destructive Testing / J. Blitz. — Springer Netherlands, 1997. — 261 p.

4 Ida N. Numerical Modeling for Electromagnetic Non-Destructive Evaluation / N. Ida. — Springer US, 1995. — 511 p.

5 Михеев М.Н. Магнитные методы структурного анализа и неразрушающего контроля / М.Н. Михеев, Э.С. Горкунов. — М.: Наука, 1993. — 266 с.

6 Ficilli F. Non-Destructive Testing by Magnetic Techniques / F. Ficilli. — LAP Academic Publishing, 2012. — 140 p.

7 Yurov V.M. X-ray computed tomography-based analysis of impact damage propagation in composite materials / V.M. Yurov, V.I. Goncharenko, S.L. Vasiliev, S.A. Dmitriev, S.A. Yurgenson // Eurasian Phys. Tech. J. — 2019. — V. 16(2). — P. 31–35.

8 Surzhikov A.P. Influence of solid-phase ferritization method on phase composition of lithium-zinc ferrites with various concentration of zinc / A.P. Surzhikov, A.M. Pritulov, E.N. Lysenko, A.N. Sokolovskii, V.A. Vlasov, E.A. Vasendina // Journal of Thermal Analysis and Calorimetry. — 2012. — V. 109. — No. 1. — P. 63–67.

9 Carnì D.L. Damage analysis of concrete structures by means of acoustic emissions technique / D.L. Carnì, C. Scuro, F. Lamonaca, R.S. Olivito, D. Grimaldi // Compos. Part B: Engineering. — 2017. — V. 115. — 79–86.

10 Yamada I. Electromagnetic and acoustic emission associated with rock fracture / I. Yamada, K. Masuda, H. Mizutani // Phys. Earth Planet. Int. — 1989. — V. 57(1–2). — P. 157–168.

11 Nazarov K.M. Study of water infiltration into cement-based mortars using real-time thermal neutron radiography / K.M. Nazarov, S.E. Kichanov, A. El Abd, M. Taman, D.P. Kozlenko // Eurasian Phys. Tech. J. — 2020. — V. 17(1). — P. 39–45.

12 O'Keefe S.G. A mechanism for the production of electromagnetic radiation during fracture of brittle materials / S.G. O'Keefe, D.V. Thiel // Phys. Earth Planet. Int. — 1995. — V. 89(11). — P. 127–135.

13 Dann D.D. Changes in the Parameters of the Electromagnetic Response of Model Dielectric Samples with Air Cavity Defects under External Deterministic Acoustic Impact / D.D. Dann, M.V. Petrov, P.I. Fedotov, E.A. Sheveleva // Bulletin of the University of Karaganda-Physics. — 2021. — V.101(1). — P. 12–17.

14 Lacidogna G. Acoustic and electromagnetic emissions as precursor phenomena in failure processes / G. Lacidogna, A. Carpinteri, A. Manuello, G. Durin, A. Schiavi, G. Niccolini, A. Agosto // Strain. — 2010. — V. 47. — P. 144–152.

15 Fursa T.V. Theoretical investigations of the influence of defects under pulsed mechanical excitation of concrete / T.V. Fursa, B.A. Lyukshin, G.E. Utsyn // Russian Physics Journal. — 2015. — V. 57(12). — P. 1658–1661.

16 Kyriazopoulos A. Non-destructive evaluation of cement-based materials from pressure-stimulated electrical emission. Preliminary results. / A. Kyriazopoulos, C. Anastasiadis, D. Triantis, C.J. Brown // Construction and Building Materials. — 2011. — V. 29(4). — P. 1980–1990.

17 Koktavy P. Experimental study of electromagnetic emission signals generated by crack generation in composite materials / P. Koktavy // Measurement Science and Technology. — V. 20(1). — 015704.

18 Stergiopoulos C. Electrical and Acoustic Emissions in cement mortar beams subjected to mechanical loading up to fracture / C. Stergiopoulos, I. Stavrakas, G. Hloupis, D. Triantis, F. Vallianato // Engineering Failure Analysis. — V. 35. — 454–461.

19 Bespal'ko A.A. Transformation of acoustic pulses into electromagnetic response in stratified and damaged structures / A.A. Bespal'ko, Y.N. Isaev, L.V. Yavorovich // J. Min. Sci. — 52(2). — P. 279–285.

20 Bespal'ko A.A. Modelling of Infrared Glow in Rock Holes / A.A. Bespal'ko, V.A. Shtirts, P.I. Fedotov, A.O. Chulkov, L.V. Yavorovich // J. Nondestr. Eval. — 2019. — V. 38. — P. 30–29.

21 Fursa T.V. Experimental and theoretical investigation of the characteristics of an electric response to an elastic impact excitation of piezo-containing heterogeneous materials / T.V. Fursa, B.A. Lyukshin, G.E. Utsyn // Russian Journal of Nondestructive Testing. — V.47(10). — P. 675–679.

22 Bespal'ko A.A. Modelling Acoustic–Electric Nondestructive Testing for Defects in Dielectric Materials / A.A. Bespal'ko, A.P. Surzhikov, D.D. Dann, G.E. Utsyn, M.V. Petrov, E.K. Pomishin // Rus. J. Nondestr. Test. — 2021. — V. 57(2). — P. 85–95.

23 X-ray flat panel detector PerkinElmer XRD 0822 [Electronic resource]. — Access mode: www.perkinelmer.com.

24 Immittance's meter LCR-819 [Electronic resource]. — Access mode: www.electronpribor.ru/catalog/53/lcr-819.htm#specification

25 Королев В.М. Апериодический пьезодатчик для ультразвуковых дефектоскопов / В.М. Королев // Дефектоскопия. — 1973. — № 4. — С. 12–18.

26 Installation guide BNC-2120 [Electronic resource]. — Access mode: https://www.ni.com/pdf/manuals/372123d.pdf

27 Warming R.F. Non-central difference schemes of the II and III order of accuracy for solving nonlinear hyperbolic equations / R.F. Warming, P. Kutler, G. Lomax // Rocket Technol. Cosmonautics. — 1973. — V. 11(2). — P. 76–85.

28 Barashkov V.N. Predicting the destruction of industrial installations / V.N. Barashkov, A.V. Gerasimov, B.A. Lyukshin // Russian Physics Journal. — 1998. — No. 10. — P. 657–661.

29 Bespal'ko A.A. Investigation and control of magnetization of magnetite ore samples by electromagnetic signal parameters / A.A. Bespal'ko, P.I. Fedotov, L.V. Yavorovich // Test. Diagn. — 2013. — No. 13. — P. 221–224.

А.А. Беспалько, Д.Д. Данн, М.В. Петров, Е.К. Помишин

Цемент-құм және цемент-шыны модельдік үлгілерінің ақауын акустикалық-электрлік тестілеу

Цемент-құм және цемент-шыны қоспаларының диэлектрлік үлгілерінің ақауларын акустикалық-электрлік тестілеудің кешенді әдісі талқыланған. Мақалада қатты күйдегі қосылыстар түріндегі ақаулары бар модельдік үлгілердің импульсті детерминирленген акустикалық қозуы кезінде электромагниттік дабылдардың параметрлері мен олардың спектрлерінің өзгеруін зерттеу нәтижелері қарастырылды. Детерминирленген акустикалық импульспен қозған кезде ақаулы диэлектрлік модельдік үлгінің кернеулі-деформацияланған күйінің уақыттық өзгеруінің математикалық есептеулерінің нәтижелері келтірілген. Сынақ объектісінің акустикалық қозу параметрлері мен магнит өрісіндегі осындай әсерге электромагниттік дабыл арасындағы байланыс көрсетілген. Зерттеу барысында цемент-құм және цемент-шыны қоспаларының электрлік кедергісі айтарлықтай ерекшеленетіні анықталды. Қос электр қабаттарының акустикалық импульстарының қозуы электромагниттік дабылдың шығарылуына әкеледі, оның параметрлері акустикалық әсер ету параметрлерімен, сондай-ақ материалдың акустикалық және электрлік қасиеттерімен анықталады. Нәтижесінде, егер қоспаның меншікті кедергісі азайтылса, онда оның өткізгіштігі артады, детерминирленген акустикалық импульстің таралуын сандық есептеу пайдаланылған үлгінің қоспасының кедергісінен өзгеше акустикалық кедергісі бар ақаудан өткен кезде оның параметрлерінің өзгеруін көрсетті.

Кілт сөздер: беріктік бақылау, диэлектриктер, акустикалық әсер, электромагниттік эмиссия, магнит өрісі, модельдеу.

А.А. Беспалько, Д.Д. Данн, М.В. Петров, Е.К. Помишин

Акустико-электрическое тестирование дефектности цементно-песчаных и цементно-стекольных модельных образцов

Обсужден комплексный метод акустико-электрического тестирования дефектности диэлектрических образцов из цементно-песчаной и цементно-стекольной смесей. Рассмотрены результаты исследований изменения параметров электромагнитных откликов и их спектров при импульсном детерминированном акустическом возбуждении модельных образцов с дефектами в виде твердотельных включений. Представлены результаты математических расчетов изменения во времени напряженно-деформированного состояния дефектного диэлектрического модельного образца при его возбуждении детерминированным акустическим импульсом. Показана связь параметров акустического возбуждения объекта тестирования и электромагнитного отклика на такое воздействие в магнитном поле. В процессе исследований установлено, что удельные электрическое сопротивление цементно-песчаной и цементно-стекольной смесей существенно отличается. Возбуждение акустическими импульсами двойных электрических слоев приводит к излучению электромагнитного сигнала, параметры которого определяются параметрами акустического воздействия, а также акустическими и электрическими свойствами материала. В результате, если уменьшить удельное сопротивление смеси, то увеличится ее проводимость. Численный расчет распространения детерминированного акустического импульса показал изменение его параметров при прохождении через дефект с отличающимся акустическим импедансом от импеданса используемой смеси образца.

Ключевые слова: неразрушающий контроль, диэлектрики, акустическое воздействие, электромагнитная эмиссия, магнитное поле, моделирование.

References

1   Mason, W.P. (1964). *Physical Acoustics. V. 1.* New York: Academic Press.

2   Klyuev, V.V. (2008). *Nerazrushaiushchii kontrol [Non-Destructive Testing].* Moscow: Mashinostroenie [in Russian].

3   Blitz, J. (1997). *Electrical and Magnetic Methods of Non-destructive Testing.* Springer Netherlands.

4   Ida, N. (1995). *Numerical Modeling for Electromagnetic Non-Destructive Evaluation.* Springer US.

5   Mikheev, M.N. & Gorkunov, E.S. (1993). *Magnitnye metody strukturnogo analiza i nerazrushaiushchego kontrolia [Magnetic methods of structural analysis and non-destructive testing].* Moscow: Nauka [in Russian].

6   Ficilli, F. (2012). *Non-Destructive Testing by Magnetic Techniques.* LAP Lambert Academic Publishing.

7   Yurov, V.M., Goncharenko, V.I., Vasiliev, S.L., Dmitriev, S.A., & Yurgenson, S.A. (2019). X-ray computed tomography-based analysis of impact damage propagation in composite materials. *Eurasian Phys. Tech. J.*, 16(2), 31–35.

8 Surzhikov, A.P., Pritulov, A.M., Lysenko, E.N., Sokolovskii, A.N., Vlasov, V.A., & Vasendina, E.A. (2012) Influence of solid-phase ferritization method on phase composition of lithium-zinc ferrites with various concentration of zinc. *Journal of Thermal Analysis and Calorimetry*. V. 109, No. 1, pp. 63–67.

9 Carnì, D.L., Scuro, C., Lamonaca, F., Olivito, R.S., & Grimaldi, D. (2017). Damage analysis of concrete structures by means of acoustic emissions technique. *Composites Part B: Engineering*. 115, 79–86.

10 Yamada, I., Masuda, K., & Mizutani, H. (1989). Electromagnetic and acoustic emission associated with rock fracture. *Phys. Earth Planet. Int.*, 57.

11 Nazarov, K.M., Kichanov, S.E., El Abd, A., Taman, M., & Kozlenko, D.P. (2020). Study of water infiltration into cement-based mortars using real-time thermal neutron radiography. *Eurasian Phys. Tech. J.*, 17(1), 39–45.

12 O'Keefe, S.G., & Thiel, D.V. (1995). A mechanism for the production of electromagnetic radiation during fracture of brittle materials. *Phys. Earth Planet. Int.*, 89(11), 127–135.

13 Dann, D.D., Petrov, M.V., Fedotov, P.I., & Sheveleva, E.A. (2021). Changes in the Parameters of the Electromagnetic Response of Model Dielectric Samples with Air Cavity Defects under External Deterministic Acoustic Impact. *Bulletin of the University of Karaganda-Physics,* 101(1), 12–17.

14 Lacidogna, G., Carpinteri, A., Manuello, A., Durin, G., Schiavi A., Niccolini G., et al. (2010). Acoustic and electromagnetic emissions as precursor phenomena in failure processes. *Strain*, 47, 144–152.

15 Fursa, T.V., Lyukshin, B.A., & Utsyn, G.E. (2015). Theoretical investigations of the influence of defects under pulsed mechanical excitation of concrete. *Russian Physics Journal*, 1658–1661.

16 Kyriazopoulos, A., Anastasiadis, C., Triantis, D., & Brown, C.J. (2011). Non-destructive evaluation of cement-based materials from pressure-stimulated electrical emission. Preliminary results. *Construction and Building Materials*, 29(4), 1980–1990.

17 Koktavy, P. (2009). Experimental study of electromagnetic emission signals generated by crack generation in composite materials. *Measurement Science and Technology*, 20(1), 015704.

18 Stergiopoulos, C., Stavrakas, I., Hloupis, G., Triantis, D., & Vallianato, F. (2013). Electrical and Acoustic Emissions in cement mortar beams subjected to mechanical loading up to fracture. *Engineering Failure Analysis* 35, 454–461.

19 Bespal'ko, A.A., Isaev, Y.N., & Yavorovich, L.V. (2016). Transformation of acoustic pulses into electromagnetic response in stratified and damaged structures. *J. Min. Sci.*, 52(2), 279–285.

20 Bespal'ko, A.A., Shtirts, V.A., Fedotov, P.I., Chulkov, A.O., & Yavorovich, L.V. (2019). Modelling of Infrared Glow in Rock Holes. *J. Nondestr. Eval.*, 38, 30–29.

21 Fursa, T.V., Lyukshin, B.A., & Utsyn, G.E. (2011). Experimental and theoretical investigation of the characteristics of an electric response to an elastic impact excitation of piezo-containing heterogeneous materials. *Russian Journal of Nondestructive Testing*. 47 (10), 675–679.

22 Bespal'ko, A.A., Surzhikov, A.P., Dann, D.D., Utsyn, G.E., Petrov, M.V., & Pomishin, E.K. (2021) Modelling Acoustic–Electric Nondestructive Testing for Defects in Dielectric Materials. *Russian Journal of Nondestructive Testing*, 57(2), 85–95.

23 X-ray flat panel detector PerkinElmer XRD 0822. *perkinelmer.com.* Retrieved from www.perkinelmer.com

24 Immittance's meter LCR-819. *electronpribor.ru.* Retrieved from www.electronpribor.ru/catalog/53/lcr-819.htm#specification

25 Korolev, V. M. (1973). Aperiodicheskii pezodatchik dlia ultrazvukovykh defektoskopov [Aperiodic piezoelectric sensor for ultrasonic flaw detectors]. *Defectoscopy*, 4, 12–18 [in Russian].

26 Installation guide BNC-2120. *ni.com.* Retrieved from https://www.ni.com/pdf/manuals/372123d.pdf

27 Warming, R.F., Kutler, P., & Lomax, G. (1973). Non-central difference schemes of the II and III order of accuracy for solving nonlinear hyperbolic equations. *Rocket Technol. Cosmonautics*, 11(2), 76–85.

28 Barashkov, V.N., Gerasimov, A.V., & Lyukshin, B.A. (1998). Predicting the destruction of industrial installations. *Russian Physics Journal,* 10, 657–661.

29 Bespal'ko, A.A., Fedotov, P.I., & Yavorovich, L.V. (2013). Investigation and control of magnetization of magnetite ore samples by electromagnetic signal parameters. *Test. Diagn.*, 13, 221–224.